Supporting Information

Detection of Pre-Malignant Gastrointestinal Lesions Using Surface-Enhanced Resonance Raman Scattering-Nanoparticle Endoscopy

Authors

Stefan Harmsen[†‡§#], Stephan Rogalla[‡§#], Ruimin Huang[†], Massimiliano Spaliviero[‖], Volker Neuschmelting[†⊥], Yoku Hayakawa[▽], Yoomi Lee[▽], Yagnesh Tailor[▽], Ricardo Toledo-Crow[○], Jeon Woong Kang[◆], Jason M. Samii[†], Hazem Karabeber[†], Ryan M. Davis[§], Julie R. White[∝∂], Matt van de Rijn[÷], Sanjiv S. Gambhir[§⊕], Christopher H. Contag[‡∅⊂*], Timothy C. Wang[▽*], and Moritz F. Kircher[†∈∠∪*]

Affiliations

[†]Department of Radiology, Memorial Sloan Kettering Cancer Center, New York, New York 10065, USA

[‡]Department of Pediatrics, Stanford University, Stanford, CA, 94305, USA

[§]Department of Radiology, Stanford University, Stanford, CA, 94305, USA

[‖]Urology Service, Department of Surgery, Sidney Kimmel Center for Prostate and Urologic Cancers, Memorial Sloan Kettering Cancer Center, New York, NY 10065, USA

[⊥]Department of Neurosurgery, University Hospital Cologne, Cologne, Germany

[▽]Department of Medicine, Columbia University, New York, New York 10032, USA

[○]Research Engineering Lab, Memorial Sloan Kettering Cancer Center, New York, New York 10065, USA

[◆]Laser Biomedical Research Center, G. R. Harrison Spectroscopy Laboratory, Massachusetts Institute of Technology, Cambridge, MA, 02139, USA

[∝]Tri-Institutional Laboratory of Comparative Pathology, Memorial Sloan Kettering Cancer Center, The Rockefeller University, and Weill Cornell Medical College, New York, NY 10065, USA

[∂]Cancer Biology and Genetics Program, Memorial Sloan Kettering Cancer Center, New York, NY 10065, USA

[÷]Department of Pathology, Stanford University, Stanford, CA, 94305, USA

[⊕]Department of Bioengineering, Department of Materials Science & Engineering, Molecular Imaging Program at Stanford, Canary Center at Stanford for Cancer Early Detection, Stanford University, Stanford, CA 94305, USA

[∅]Department of Microbiology and Immunology, Stanford University, Stanford, CA, 94305, USA

[⊂]Institute of Quantitative Health Science and Engineering, Department of Biomedical Engineering, and Department of Microbiology and Molecular Genetics, Michigan State University, East Lansing, MI, 48824, USA

[∈]Center for Molecular Imaging and Nanotechnology (CMINT), Memorial Sloan Kettering Cancer Center, 1275 York Avenue, New York, New York 10065, USA

[∠]Department of Molecular Pharmacology, Memorial Sloan Kettering Cancer Center, 1275 York Avenue, New York, New York 10065, USA

[∪]Department of Imaging, Dana-Farber Cancer Institute, 450 Brookline Avenue, Boston, MA 02215

*Corresponding Authors

*Email C.H.C.: contagch@egr.msu.edu; T.C.W.: tcw21@columbia.edu; M.F.K.: moritz_kircher@dfci.harvard.edu

Supplementary Figures

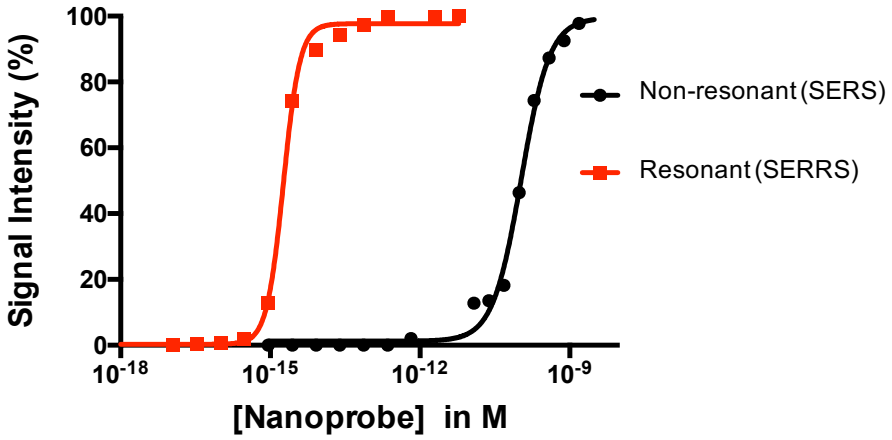

Figure S1. Detection limits of non-resonant SERS- *versus* resonant SERRS nanoparticles. A concentration series of non-resonant SERS nanoparticles (Raman reporter: trans-1,2-bis (4-pyridyl) ethylene (BPE))[1] and resonant SERRS nanoparticles (Raman reporter: IR792)[2] were measured using identical imaging settings (785-nm excitation laser; 100 mW; 1.0 s acquisition). As shown, the resonant SERRS nanoparticles demonstrated a 1000-fold lower limit of detection than the non-resonant SERS nanoparticles. At 100% the CCD detector was saturated, hence the signal plateau.

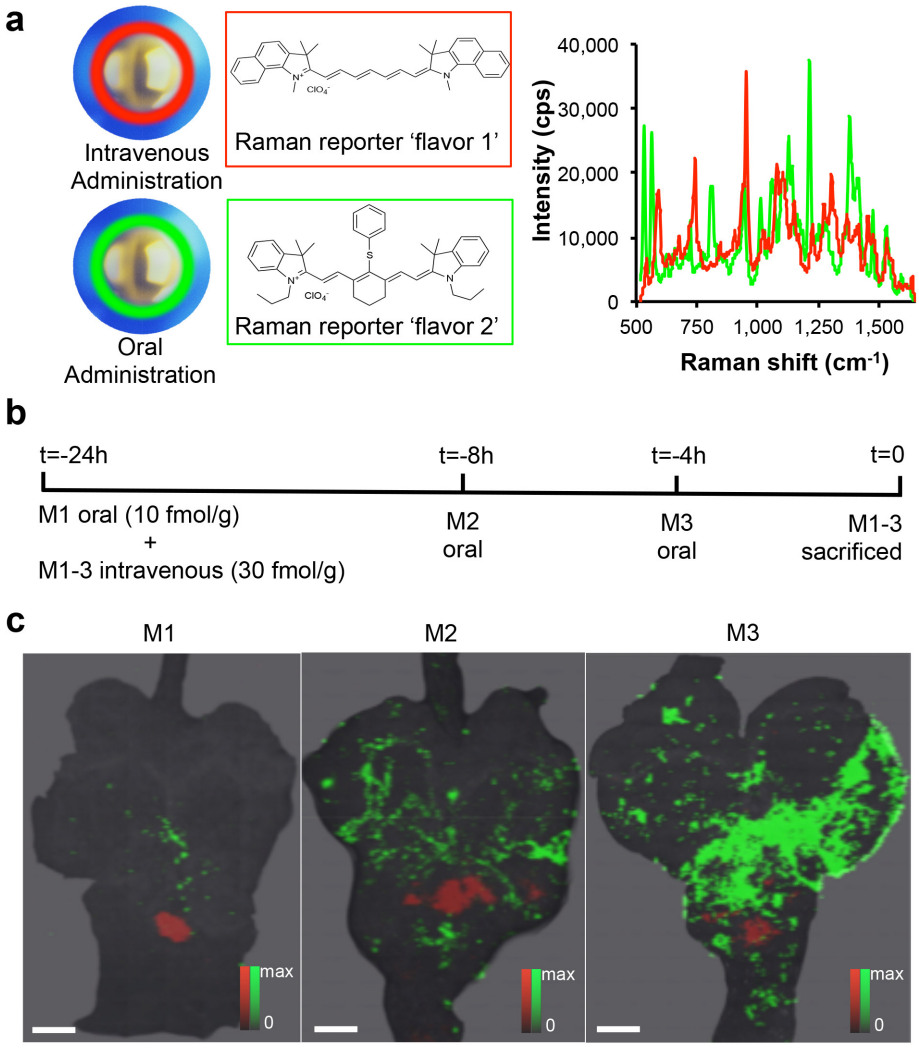

Figure S2. Evaluation of the route of SERRS nanoparticle administration. **(a)** SERRS nanoparticle schematic and associated Raman spectra. The SERRS-NPs consist of a 60-nm gold core, which is encapsulated in a 15-nm resonant Raman reporter-embedded silica shell (blue). To enable multiplexed detection, two structurally different resonant Raman reporters were used (*i.e.* IR780 perchlorate (red) and IR792 perchlorate (green), which generate very distinct Raman spectra (measured at 50-µW laser power, 1.0-s acquisition time, 5× objective). **(b)** Dosing scheme: The day prior to Raman imaging MNU-treated/*H.felis*-infected GAS-KO mice (M1-3) were intravenously injected *via* tail vein (30 fmol/g) with PEGylated SERRS nanoparticle 'flavor 1'. Mouse 1 (M1) was additionally orally gavaged to receive SERRS nanoparticle 'flavor 2' (10 fmol/g) at t=-24 hours. At t=-8 hours, mouse 2 (M2) received 10 fmol/g orally administered SERRS nanoparticle 'flavor 2'. Mouse 3 (M3) received orally administered SERRS nanoparticle 'flavor 2' 4 hours prior to Raman imaging. The mice were sacrificed *via* CO_2 asphyxiation and the stomachs were harvested. The stomachs were opened along the greater curvature and scanned by Raman imaging (785-nm laser wavelength, 10-mW laser power, 1.5-s acquisition time, and 5× objective). **(c)** The Raman spectra of both SERRS-NPs 'flavor 1 and 2' were unmixed *via* a direct classical least square (DCLS) algorithm using Wire 3.4 software (Renishaw). The intravenously administered SERRS nanoparticle 'flavor 1' (red) highlighted focal lesions in the pyloric antrum, while orally administered SERRS nanoparticle 'flavor 2' (green) were non-specifically adsorbed by the gastric mucosa (scale bar, 2 mm). Therefore, the intravenous route was used for SERRS nanoparticle administration.

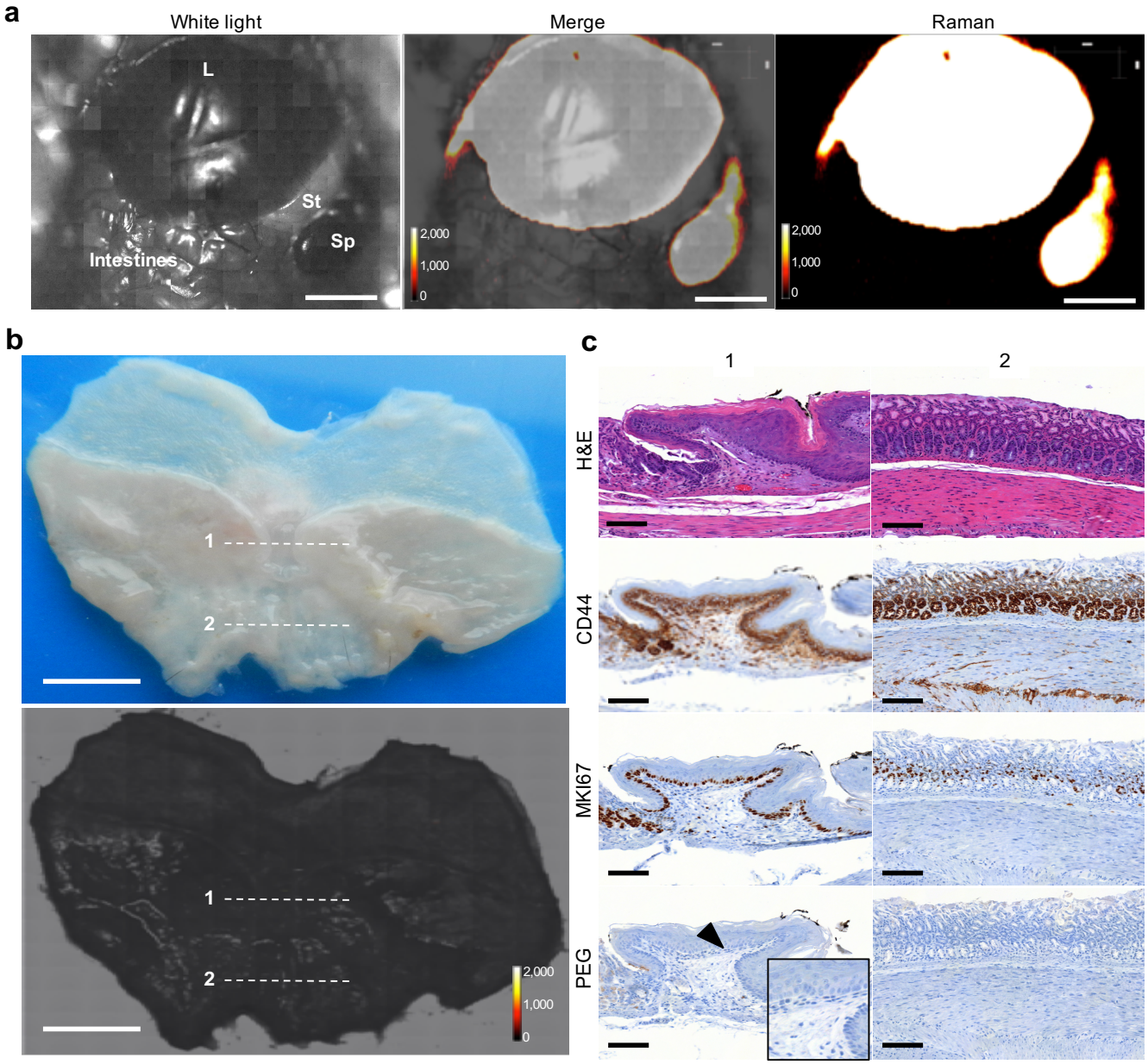

Figure S3. Biodistribution of intravenously injected SERRS-NPs in healthy control wild-type animals. (a) *In situ* Raman imaging of SERRS NP biodistribution 18 hours post i.v. administration (dose 30 fmol/g) in an age-matched C57BL/6 control animal (L=liver; St=stomach; Sp=spleen). All scale bars, 5 mm. **(b)** A stomach of an age-matched C57BL/6 control animal (*n* = 4) injected with SERRS-NPs (30 fmol/g) was opened along the greater gastric curvature. Upon Raman imaging, no significant SERRS nanoparticle signal was observed at the gastroesophageal junction (GEJ; 1) or at the pyloric antrum (2; scale bars, 5 mm). **(c)** H&E and immunohistochemical staining of transverse tissue sections of the GEJ (1) and pyloric antrum (2). The tissue at the GEJ and pyloric antrum appear normal on H&E. As expected, CD44 and Ki-67 (MKI67) are confined to the proliferative basal region of the epithelium at the GEJ (1), and to the lower glandular region or glandular necks, respectively, at the pyloric antrum (2). The SERRS nanoparticle (PEG) immunostaining was negative for all sections confirming that the SERRS-NPs did not accumulate in normal tissues. The inset shows a higher magnification (4×) and demonstrates the lack of granular staining in a representative focus (black arrowhead). The brownish stain on the left part of the control group (Figure S2B-1-PEG) on the left is not granular and thus is non-specific immunostaining that does not reflect the presence of PEGylated SERRS nanoparticles or aggregates thereof. All scale bars in panels **(b)** and **(c)**, 100 μm.

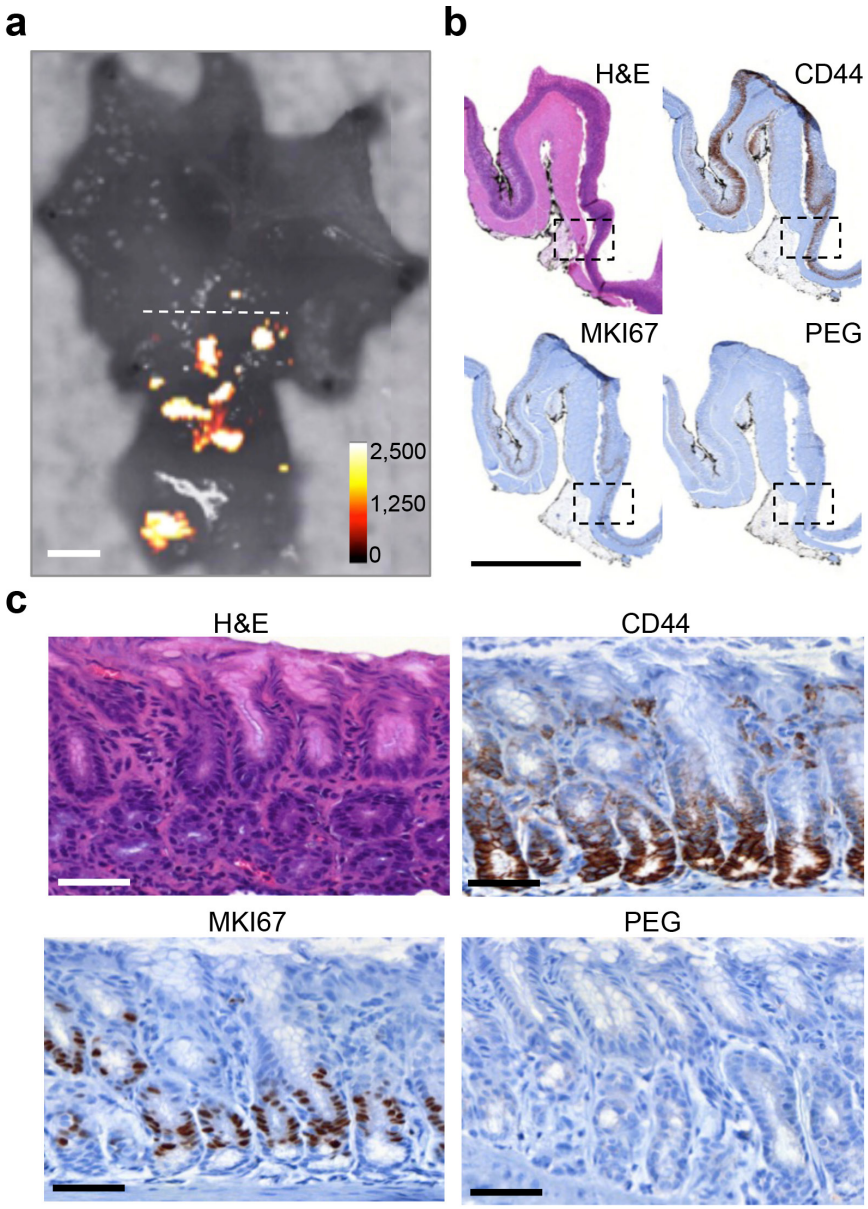

Figure S4. Histological evaluation of SERRS-negative area in *Helicobacter felis*-infected/MNU-treated GAS-KO mouse. **(a)** SERRS negative area (dotted line) was sectioned transversely (scale bar, 5 mm). (**b)** Overview (scale bar, 2 mm), and, (**c)** Higher magnification (20×) views of the immunohistochemical sections (arrow-head) that were stained for CD44, MKI67 and polyethylene glycol (PEG; polymer on the surface of the SERRS nanoparticle). CD44 and MKI67 expression are focally expressed at the proliferative region of the epithelium (scale bars, 50 μm). This, in combination with normal cellular organization (H&E) and the lack of anti-PEG staining demonstrates that the sectioned SERRS-negative area is normal gastric tissue.

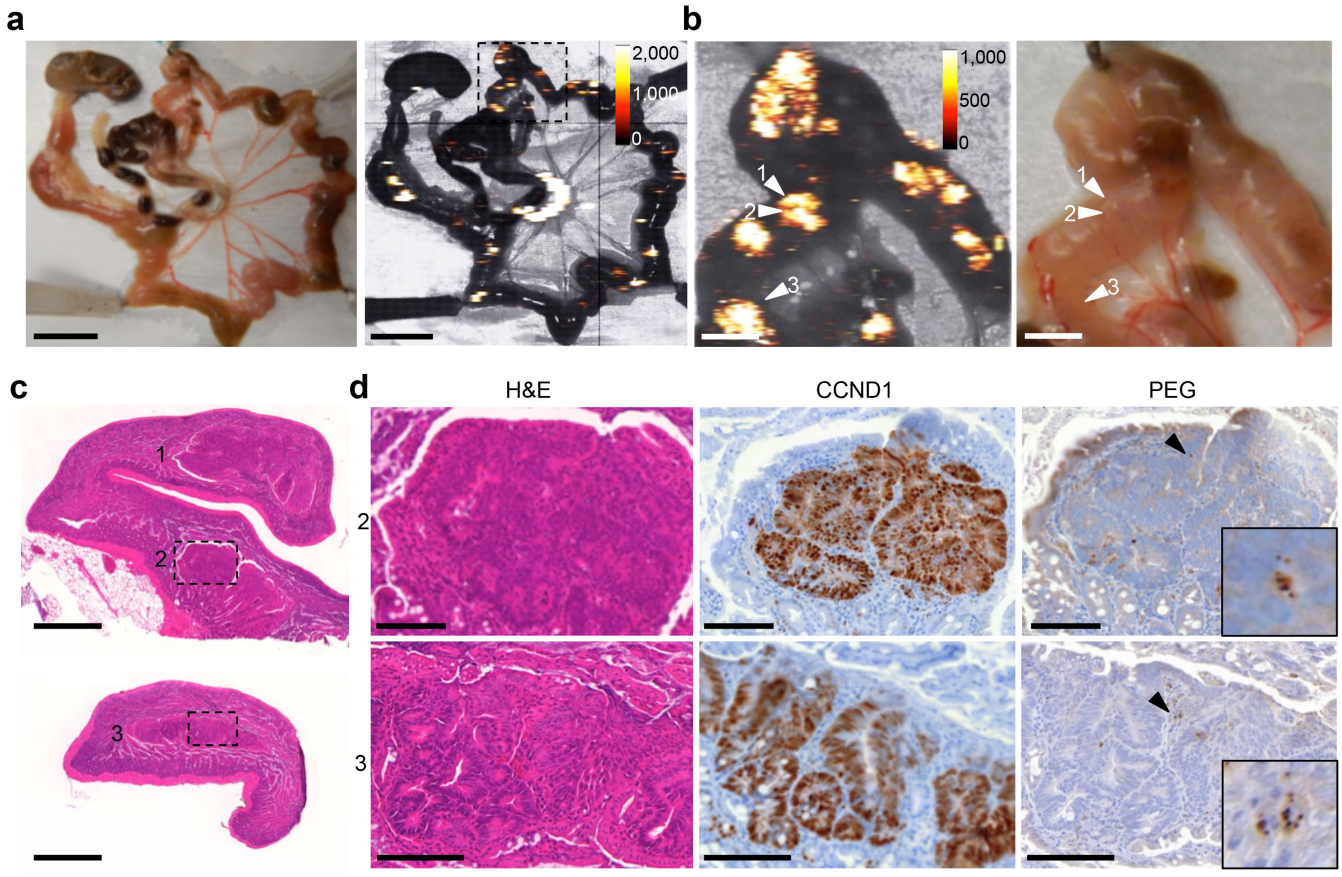

Figure S5. SERRS nanoparticle-mediated detection of adenoma in a symptomatic Apc$^{Min/+}$ mouse. (**a)** Photo and Raman image of an intestinal section of an Apc$^{Min/+}$ mouse that was injected with SERRS-NPs 18 hours before sacrifice. As shown, multiple SERRS-positive lesions were identified (signal intensity in counts per second; scale bar, 5 mm). The indicated area was rescanned at a higher magnification and higher resolution. (**b**) Higher resolution Raman image of the selected area. Multiple discrete SERRS positive lesions were detected (signal intensity in counts per second; scale bar, 2 mm). Transverse sectioning was performed along the indicated lines and the sections were examined by histology. (**c)** Lower magnification micrograph of the cyclin D1 (CCND1) immunostained sections 1, 2, and 3 (scale bar, 1 mm), which demonstrates that CCND1 expression corresponds well with SERRS positivity in panel (**b**). **(d)** Higher magnifications of the H&E-, CCND1- and PEG (immuno)stained lesions indicated by the dashed boxes in sections 2 and 3 (scale bars, 100 µm). At higher magnification, the granular PEG immunostaining was observed within the CCND1 positive sections confirming the specific accumulation of PEGylated SERRS-NPs in the adenomatous polyps. Insets show a higher magnification (8×) of the area indicated by the arrowheads.

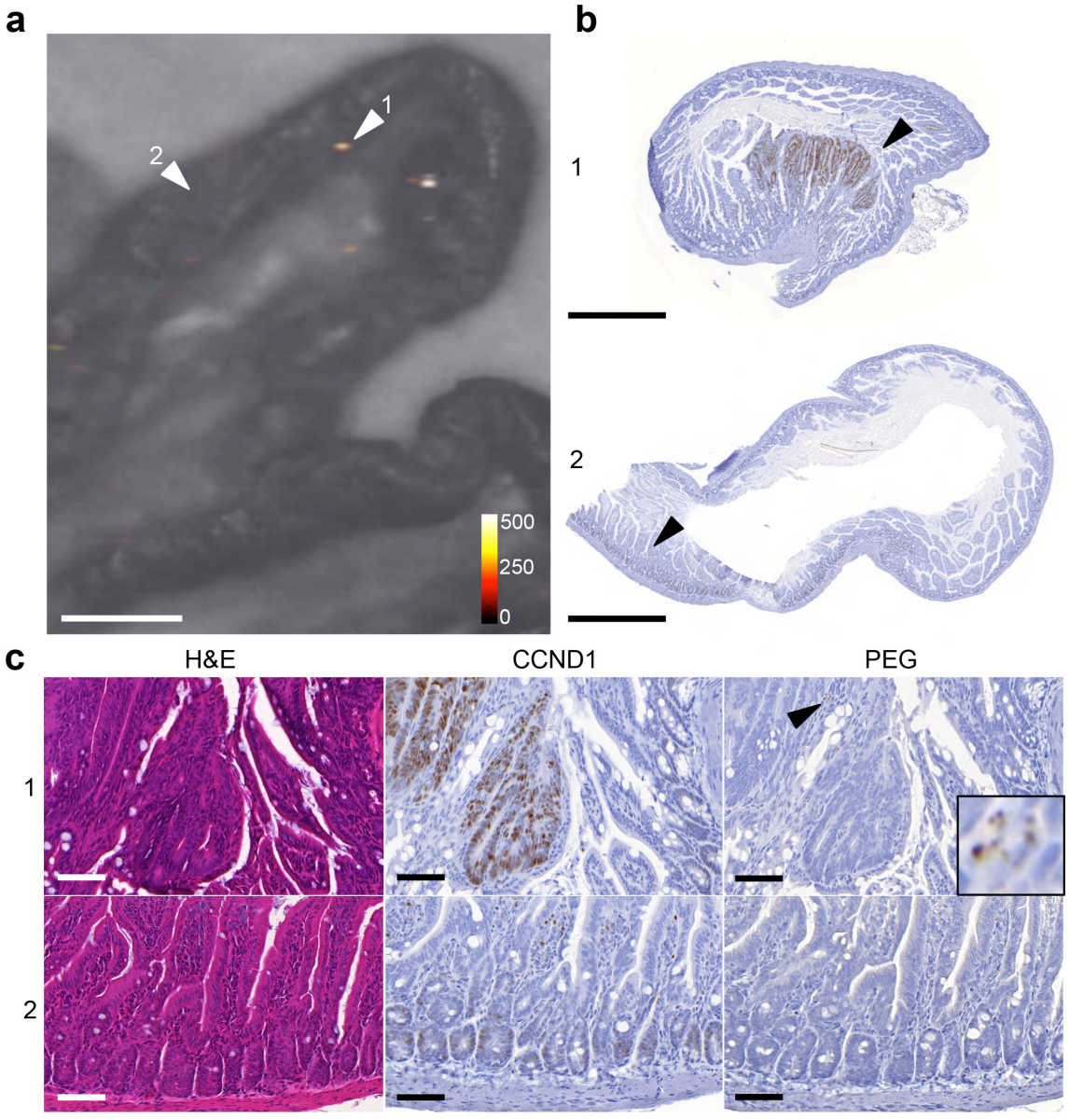

Figure S6. SERRS-guided biopsy of early adenoma in asymptomatic Apc$^{Min/+}$mouse. (**a**) The intestine of an asymptomatic Apc$^{Min/+}$ mouse that was tail-vein injected with SERRS-NPs (30 fmol/g) was scanned by Raman (intensity in counts per second). A few microscopic SERRS positive lesions were identified (arrowhead 1; scale bar 2 mm). (**b)** Low magnification overview of histological sections 1 and 2 that were stained for the tumor marker CCND1. **c,** Higher magnification of the areas indicated by arrowhead 1 and 2 in panel (**b**). Section 1 was positive for the tumor marker CCND1 and PEG (SERRS nanoparticle stain) and was graded dysplastic (Inset shows 4× magnifications of the areas indicated by the arrow head; scale bars, 500 μm). The SERRS-negative, control section 2 demonstrated normal tissue architecture and was negative for CCDN1 and SERRS nanoparticle marker (PEG) staining.

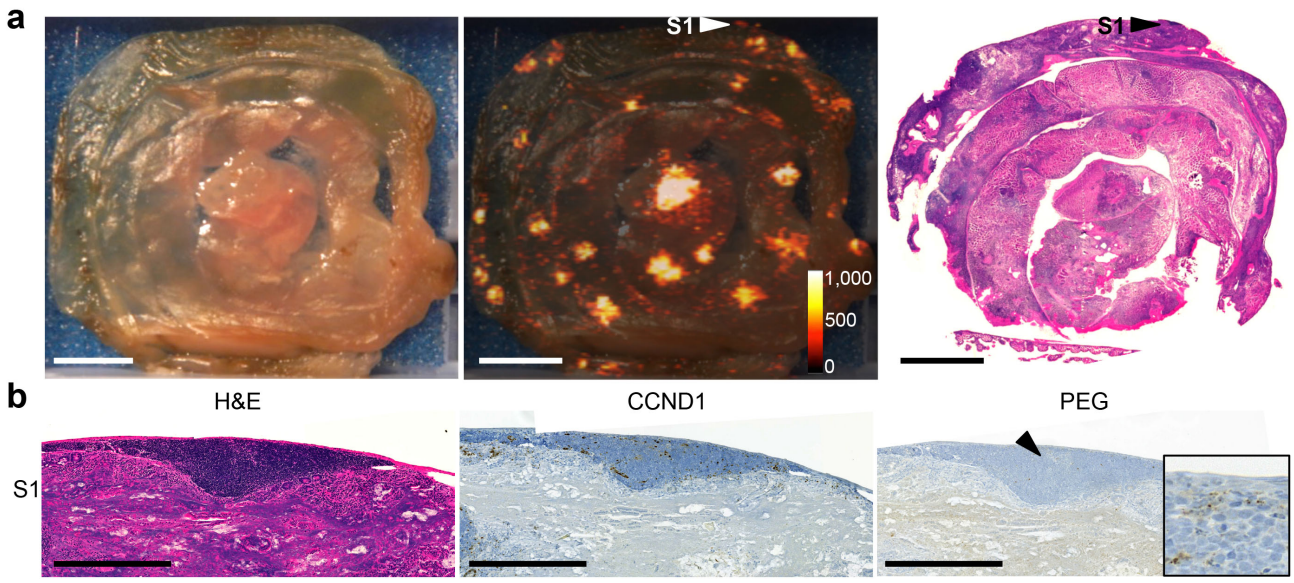

Figure S7. Example of a false positive lesion in the intestinal tract of Apc$^{Min/+}$ mice. (**a**) A segment of the small intestine of an Apc$^{Min/+}$ mouse that was injected with SERRS-NPs was scanned by Raman imaging *ex vivo* (intensity in counts per second). All scale bars, 5 mm. (**b**) 5-µm thick tissue sections were stained with H&E or for CCND1 or PEG. The SERRS positive lesions were correlated to histologic appearance and CCND1 status. α-PEG was used to corroborate the presence of the SERRS-NPs. One of the SERRS-positive lesions (indicated by arrowhead S1) turned out to be gut-associated lymphoid tissue (GALT). Scale bars, 1 mm. Inset shows 4×-magnifications of the areas indicated by the arrowhead. See also **Fig. 5** and **Table 1**.

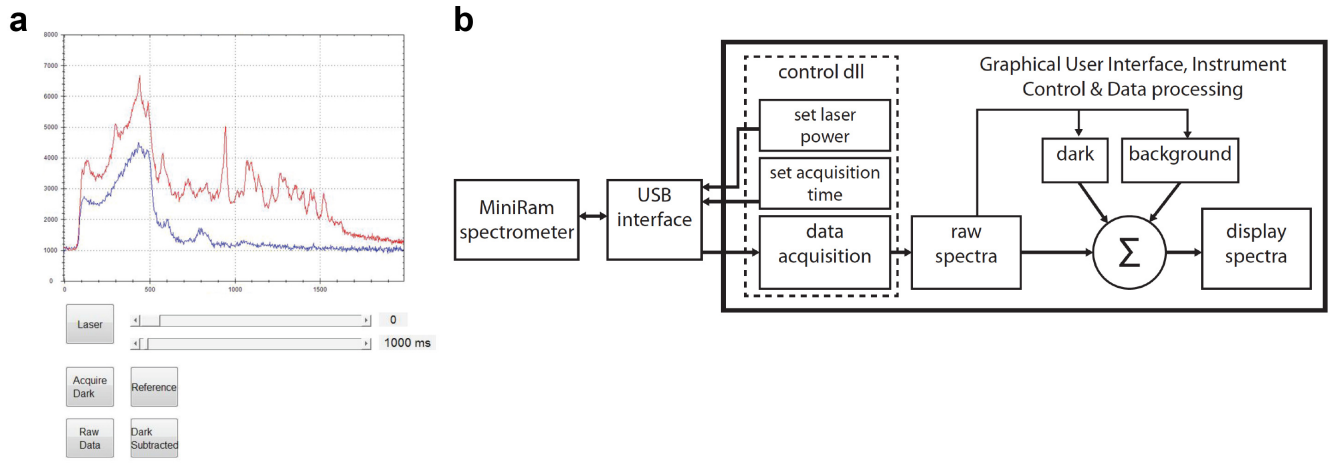

Figure S8. Graphical User Interface (GUI), Instrument Control & Data Processing of the mouse Raman fiberscope. (a) The simplified GUI allows laser on/off, intensity control and acquisition integration time. Push buttons move the spectra to the dark and background arrays. Toggle buttons select the state of displayed spectra with dark subtracted, background subtracted or both. For operation: laser intensity and integration time are selected through preliminary measurements. Once established, the dark spectrum is acquired before laser is turned on. The laser is switched on, and the background spectra are acquired before probing the sample. Dark- and background subtraction are selectively enabled on the displayed spectrum. If the integration time is modified the dark spectrum is discarded. If either of the controls are modified, the background spectrum is discarded and must be reacquired. **(b)** The software was developed in Matlab with dynamic link libraries (dll) from B&WTek for the instrument control. The background and dark spectra are stored in the static arrays and the accumulator subtracts them from incoming spectra before display.

Supplementary References

(1) Kircher, M. F.; de la Zerda, A.; Jokerst, J. V.; Zavaleta, C. L.; Kempen, P. J.; Mittra, E.; Pitter, K.; Huang, R.; Campos, C.; Habte, F.; Sinclair, R.; Brennan, C.; Mellinghoff, I. K.; Holland, E. C.; Gambhir, S. S., A Brain Tumor Molecular Imaging Strategy Using a New Triple-Modality MRI-Photoacoustic-Raman Nanoparticle. *Nat. Med.* **2012,** *18*, 829-34.

(2) Harmsen, S.; Bedics, M. A.; Wall, M. A.; Huang, R.; Detty, M. R.; Kircher, M. F., Rational Design of a Chalcogenopyrylium-based Surface-Enhanced Resonance Raman Scattering Nanoprobe with Attomolar Sensitivity. *Nat. Commun.* **2015,** *6*, 6570.